ISSN 0915-6364

NATIONAL INSTITUTE FOR FUSION SCIENCE

Validity of n^{-3} Scaling Law in Dielectronic Recombination Processes

J.G. Wang, T. Kato and I. Murakami

(Received - Mar. 2, 1999)

NIFS-DATA-52 Apr. 1999

RESEARCH REPORT
NIFS-DATA Series

NAGOYA, JAPAN

Validity of n^{-3} scaling law in dielectronic recombination processes

J.G. Wang, T. Kato, and I. Murakami

April 11, 1999

Abstract

In the frame of quantum defect theory, a Simplified Relativistic Configuration Interaction (SRCI) method is developed to study the Dielectronic Recombination (DR) processes. In this method, the infinite resonant doubly excited states involving high Rydberg state can be treated conveniently in a unified mannar by interpolation. This provides an efficient method to check the validity of extrapolation based on n^{-3} scaling law, which is widely used to treat the DR processes involving high Rydberg states. As an example, we studied the DR processes for Li-like argon, and the results are compared with the scaling laws and the experimental measurements, respectively.

Keyword: dielectronic recombination, simplified relativistic configuration interaction method, n^{-3} scaling law, Li-like argon

1. Introduction

Dielectronic Recombination (DR) can be regarded as a resonant radiative recombination process. As a free electron with a specific kinetic energy collides with an ion A^{q+}, one of the bound electrons of the ion A^{q+} is excited from the initial $n_i l_i$ orbital into the $n_f l_f$ orbital, the free electron is then captured into an unoccupied orbital nl and forms a resonant doubly excited state; subsequently, the resonant doubly excited state decays into a non-autoionizing state through radiative transition processes. Its importance to influence the ionic balance in high temperature plasmas, such as solar corona, has been known for many years [1]. Its radiative emission is a significant contributor for plasma cooling in hot plasmas in fusion experiments. The dielectronic satellites of hydrogen-like ion have also been used to measure plasma densities in high density plasmas [2] and the electron temperatures in solar flares [3].

Many theoretical methods have been developed to calculate the DR process, such as distorted wave method [4, 5], close coupling methods [6, 7], non-relativistic single configuration[8, 9] and relativistic multi-configuration methods[10, 11]. In these calculations, it is a tedious work to obtain the accurate DR rate coefficients since they involve many resonant doubly excited high Rydberg states. Due to the difficulty of numerical calculation on wavefunction and too enormous number of high Rydberg states, most calculations either neglect high-lying doubly excited states or simply use the n^{-3} scaling law to treat them[9, 12, 13, 14]. Neglecting high-lying doubly excited states will induce inaccuracies in the DR calculations, especialy for low Z atom. The evaluation by the n^{-3} scaling law can give an improvement, but it should be checked for high Rydberg states. In order to check the validity of the n^{-3} scaling law, Karim and Bhalla have performed explicit DR calculations for Rydberg states ($n \leq 8$) on heliumlike ions using the Hatree-Fock atomic model [15], and found that the $1/n^3$ scaling law is appropriate when $n \geq 8$. However, this conclusion isn't always correct for lower Z ions, we will discuss it in section 3.

In fact, Quantum Defect Theory (QDT) has been developed to treat the atomic processes involving high Rydberg states [16, 17, 18], which was also used to study the DR cross sections and rate coefficients for high Rydberg states by extrapolation [7, 19, 20, 21]. Recently, in the frame of QDT, we have developed a Simplified Relativistic Configuration Interaction (SRCI) method to study the dielectronic recombination processes [22, 23, 24]. In this method, all the resonant doubly excited high Rydberg states are classified into different channels with same angular momentum quantum number and same angular momentum coupling type. In each channel, the defined energy-normalized matrix elements vary smmothly with the energy of high Rydberg states. Only a few points (including a continuum point) are calculated, the many resonant high Rydberg states can be treated in an unified manner by interpolation (rather than extrapolation), and then the DR cross sections and rate coefficients can be obtained conveniently. This method gives an overall description of all high Rydberg states in a channel, and avoid the inaccuracies of extrapolation through one point. By analyzing the energy-normalized matrix elements in a small energy domain, we can check the validity of n^{-3} scaling law.

In this paper, as an example, we studied the DR processes of $\Delta N = 0$ transition for Li-like argon. The DR processes has the form

$$e^- + Ar^{15+}(1s^2 2s) \quad \rightarrow \quad Ar^{14+}(1s^2 2pnl)^{**}$$

$$\rightarrow \begin{cases} Ar^{14+}(1s^2 2snl)^* + h\nu \\ Ar^{14+}(1s^2 2pn'l')^* + h\nu. \end{cases} \quad (1)$$

Due to energy conservation, the possible resonant doubly excited states appear at high Rydberg states ($n \geq 10$). It provide a good example to check the validity of n^{-3} scaling law for high Rydberg states. The results on SRCI method are compared with the scaling laws and the experimental measurements, repectively.

2. Theoretical Method

The cross section of resonant capture processes, in which the Ar^{15+} ion in initial state $i(1s^2 2s)$ captures a free electron with a specific energy ϵ_i and forms the Ar^{14+} ion in the resonant doubly excited state $j(1s^2 2pnl)$, can be treated in the isolated resonance approximation (atomic unit is used throughout unless specified),

$$\sigma_{ij}^c = \frac{\pi^2 \hbar^3}{m_e \epsilon_i} \frac{g_j}{2g_i} A_{ji}^a \cdot \delta(\epsilon - \epsilon_i), \quad (2)$$

where g_i and g_j are the statistical weight of the state i and j,respectively. A_{ji}^a is Auger decay rate (inverse resonant capture), which can be calculated by Fermi golden rule,

$$A_{ji}^a = \frac{2\pi}{\hbar} | < \Psi_j | \sum_{s<t} \frac{1}{r_{s,t}} | \Psi_{i\epsilon_i} > |^2, \quad (3)$$

where Ψ_j and $\Psi_{i\epsilon_i}$ are antisymmetrized many-electron wavefunctions for j state and i state plus a free electron, respectively.

We construct the configuration wavefunctions $\phi(\Gamma JM)$ (Γ denotes the configuration $1s^2 2pnl$ and parity) as antisymmetrized product-type wavefunctions from central-field Dirac orbitals with appropriate angular momentum coupling[25]. All relativistic single-electron wavefunctions (bound and continuum) are calculated based on the atomic self-consistent potential obtained from the ground-state configuration for Ar^{14+}[26, 27]. An atomic state function for the state $j(1s^2 2pnl)$ with total angular momentum JM is then expressed as linear expansion of the configuration wavefunctions with same principal quantum numbers $(2, n)$, and same orbital angular momentum quantum numbers (p, l)

$$\psi_j(JM) = \sum_{\lambda=1}^{m} C_{j\lambda} \phi(\Gamma_\lambda JM). \quad (4)$$

Here m is the number of the configuration wavefunctions and the mixing coefficients $C_{j\lambda}$ for state j are obtained by diagonalizing the relevant Hamiltonian matrices[25]. The free state is chosen as the single configuration wavefunction. Then we have

$$A_{ji}^a = \frac{2\pi}{\hbar} | \sum_{\lambda=1}^{m} C_{j\lambda} M_{ij\lambda}^a |^2, \quad (5)$$

where the Auger decay matrix element $M_{ij\lambda}^a$ is defined as

$$M_{ij\lambda}^a = < \phi(\Gamma_\lambda JM) | \sum_{s<t} \frac{1}{r_{s,t}} | \Psi_{i\epsilon_i} > . \quad (6)$$

Based on QDT, when l are fixed and n varies from bound to continuum state, all the resonant doubly excited states with same J will form a channel. In the channel, the energy-normalized matrix element can be defined as

$$\overline{M}_{ij}^a = \sum_{\lambda=1}^{m} C_{j\lambda} M_{ij\lambda}^a \cdot (\nu_n^{3/2}/q), \quad (7)$$

here (ν_n^3/q^2) is the density of state, $\nu_n = n - \mu_n$, μ_n is the corresponding quantum defect, and q equals to ionization degree of doubly excited states plus one. This energy-normalized matrix element $\overline{M}_{ij}^a$ varies smoothly with the electron orbital energy in the channel[22, 24]. When the energy-normalized matrix elements of a few states (including one continuum state) in a channel have been calculated, the Auger decay matrix elements of infinite discrete states of that channel can be obtained by interpolation. From the expression (7) and (5), the Auger rates and capture rates (by detailed balance) of the infinite resonant doubly excited states can be calculated conveniently.

The resonant doubly excited state may autoionize with a rate A_{ji}^a by reemitting Auger electron or decay radiately into a lower energy state k with a radiative rate A_{jk}^r, which is defined as

$$A_{jk}^r = \frac{4e^2\omega}{3\hbar c^3 g_j} | < \Psi_j | T^{(1)} | \Psi_k > |^2, \quad (8)$$

where ω is photon energy, $T^{(1)}$ is electronic dipole operator [22]. The atomic wavefunction Ψ_k for final state k can be constructed in the similar way as the expression (4)

$$\psi_k(J'M') = \sum_{\lambda'=1}^{m'} C_{k\lambda'} \phi'(\Gamma'_\lambda J'M'). \quad (9)$$

Then we have

$$A_{jk}^r = \frac{4e^2\omega}{3\hbar c^3 g_j} | \sum_{\lambda,\lambda'=1}^{m,m'} C_{j\lambda} C_{k\lambda'} M_{\lambda,\lambda' jk}^r |^2, \quad (10)$$

where the radiative transition matrix element is defined as

$$M_{\lambda,\lambda' jk}^r = < \phi(\Gamma_\lambda JM) | T^{(1)} | \phi'(\Gamma'_\lambda J'M') > . \quad (11)$$

For radiative process with certain final state $k(1s^2 2snl)$ or $k(1s^2 2pn'l')$, the resonant doubly excited states with the fixed (l) and different orbital energy form a channel. In the channel, the energy-normalized radiative transition matrix element is defined as

$$\overline{M}_{jk}^r = \sum_{\lambda,\lambda'=1}^{m,m'} C_{j\lambda} C_{k\lambda'} M_{\lambda,\lambda' jk}^r \cdot (\nu_n^{3/2}/q). \quad (12)$$

This energy-normalized matrix element varies slowly with the electron orbital energy[22, 29, 30, 31]. By interpolation, all the energy-normalized matrix elements of infinite discrete states in a channel can be obtained. From

the expression (10), we can obtain all the radiative rates in the channel.

The resonance energy ϵ_i can be calculated under the frozen core approximation [32]. Then, we can obtain the DR cross sections for any resonant doubly excited states conveniently,

$$\sigma_{ij;k} = \frac{\pi^2\hbar^3}{m_e\epsilon_i}\frac{g_j}{2g_i}P_{ij;k}\cdot\delta(\epsilon-\epsilon_i) \tag{13}$$

and

$$P_{ij;k} = \frac{A^a_{ji}A^r_{jk}}{\sum_{k'}A^r_{jk'}+\sum_{i'}A^a_{ji'}}. \tag{14}$$

Here the summation i' is over all possible states of Ar^{15+} ion, and the summation k' is over all possible states of Ar^{14+} whose energy are below state j.

The summation of cross sections over all possible k is expressed as

$$\sigma_{ij} = \sum_k \sigma_{ij;k}. \tag{15}$$

The DR strength S_{ij}, which is the integral of the DR cross section over the natural width of the resonance, can be written as

$$S_{ij} = \frac{\pi^2\hbar^3}{m_e\epsilon_j}\frac{g_j}{2g_i}\frac{A^a_{ji}\sum_k A^r_{jk}}{\sum_{k'}A^r_{jk'}+\sum_{i'}A^a_{ji'}}. \tag{16}$$

Using the velocity distribution of the free electron, we can obtain the dielectronic recombination rate coefficients.

3. Result and Discussion

There are enormous intermediate resonance states involved in the DR process, which makes the explicit calculations not practicable[15]. Hence, the n^{-3} scaling law is widely used in the literature to extrapolate the satellite intensity factors (proportional to DR cross section) for higher ($n \geq 4$) resonances[9, 12, 13, 14]. Based on QDT, we have developed the SRCI method, in which all the high-lying resonant doubly excited states are treated conveniently through interpolation. This method provides an overall description on the behaviors of high Rydberg states, and can be regarded as an efficient method to check the avalidity of n^{-3} scaling law. As an example, we studied the DR processes for Ar^{15+} ions, and calculated the Auger rates, radiative rates, integrated cross sections and rate coefficients. In our calculation, we have included the doubly excited states $1s^22pnl$ with $10 \leq n \leq 15, l \leq 11$ (and corresponding continuum states) as benchmark points.

A. Auger rates

Using formulae (6) and (7), we can obtain the energy-normalized Auger transition matrix elements. As an example, we plotted the energy-normalized Auger transition matrix elements $\overline{M}^a_{ji}$ for the four Auger channels in Fig.1, which include $1s^22pns(^3P_0) \rightarrow 1s^22s + \varepsilon p_{1/2}$, $1s^22pnd(^3P_0) \rightarrow 1s^22s + \varepsilon p_{1/2}$, $1s^22png(^3F_2) \rightarrow 1s^22s + \varepsilon p_{3/2}$, $1s^22pnj(^3I_{11}) \rightarrow 1s^22s + \varepsilon g_{9/2}$, and n changes from $n = 10$ to $n = \infty$ and continuum states. In each channel, $\overline{M}^a_{ji}$ vary smoothly with the orbital energy of capture electron. There are infinitely many doubly excited high Rydberg states in a small energy domain below the threshold value. When the energy-normalized matrix elements of a few states (including one continuum state) in a channel have been calculated, all the Auger matrix elements of infinitely many doubly excited states of that channel can be obtained by interpolation. From the expression (7) and (5), the Auger rates of the infinitely many resonant doubly excited states can be calculated conveniently. This method provides an overall description for high Rydberg states located in the small energy domian, which is not same as the method of widely used extrapolation by one points based on n^{-3} scaling law.

In the calculation of Auger rates for high Rydberg doubly excited states, there are two ways to extrapolate the Auger rate based on n^{-3} scaling law. One is extrapolation from the Auger rate of one Rydberg state with certain principal quantum number n_0 to these Rydberg states with higher principal quantum number n by $A^a_{ji}(n) = A^a_{ji}(n_0)\times n_0^3/n^3$[33, 34, 35]. If we assume that our energy-normalized matrix elements are constant and the quantum defects can be neglected, namely, $\overline{M}^a_{ji}(n) = \overline{M}^a_{ji}(n_0)$ and $\mu_n = 0$ when $n \geq n_0$, and then we can obtain this scaling law from eq.(7) and (5). Another way is extrapolation from the threshold value of the according partial electron-impact excitation cross sections[36, 37, 38]. Our energy-normalized matrix elements above the threshold value are just the partial electron-impact excitation matrix elements with exchange. If we assume that our energy-normalized matrix elements below threshold value are constant and equal to the threshold value in a channel, and the quantum defects can be neglected, then from eq.(7) and (5), we can obtain the n^{-3} scaling law in the references[36, 37, 38].

From above analysis, we can conclude that if the n^{-3} scaling law is well preserved, it is necessary that the energy-normalized matrix elements below threshold value are almost constant in the small energy domain where high Rydberg states are located. So we can check the validity of n^{-3} scaling law in these two extrapolations by analyzing whether the energy-normalized matrix elements in the small energy domain below the threshold value are constant in a channel. In our example, the energy-normalized matrix elements near the threshold value are almost constant in most of channels, as shown in Fig.1. This means that the n^{-3} scaling law should be well preserved for these channels. However, it can be seen that as the orbital quantum number l increases, the changing of the energy-normalized matrix elements in the small domain becomes large, so it can be expected the deviation from the n^{-3} scaling law also become large with increasing l. This can be confirmed from the Ayger rates in Fig.2 and Fig.3, which are corresponding to the four channels in Fig.1.

For $1s^22pns(^3P_0) \rightarrow 1s^22s+\varepsilon p_{1/2}$ and $1s^22pnd(^3P_0) \rightarrow 1s^22s + \varepsilon p_{1/2}$ channels, because the curve of energy-normalized matrix elements is almost constant as the

curves 1 and 2 shown in Fig.1, the results from interpolation on SRCI method and two extrapolation on n^{-3} scaling law are in agreement within a few percent as shown in Fig.2. For $1s^22png(^3F_2) \rightarrow 1s^22s + \varepsilon p_{3/2}$ channel, The difference of SRCI method and two extrapolation methods is within 15% as shown in Fig.3(a). For $1s^22pnj(^3I_5) \rightarrow 1s^22s + \varepsilon i_{11/2}$ channel, the difference approaches to 100% as shown in Fig.3(b), this is because the relative variation of $\overline{M^a}$ is large with increasing l, as shown in Fig.1. The fundmental reason is as following: for a smaller values of radial distance r, the energy-normalized wavefunctions vary slowly with orbital energy[18, 28], which implies the scaling law for Auger or radiative rate[28]. But this cann't be extend to bigger r. So the states with a relative big amplitude of wavefunction in smaller r have good scaling law. As l increases, the effect of centrifugal term becomes strong, which cause a relative big amplitude of wavefunction in bigger r. So the accuracy of n^{-3} scaling law becomes low with increasing l, as shown in Fig.2 and Fig.3. As n increases, the difference increases between interpolation on SRCI method and first type of extrapolation and decreases between interpolation and second type of extrapolation, as shown in Fig.3. This comes from the different initial points for the extrapolation.

B. Radiative rates

Here, we consider two main types of dipole transition processes, as shown in eq.(1). For $Ar^{14+}(1s^22pnl)^{**} \rightarrow Ar^{14+}(1s^22snl)^* + h\nu$ (rate is denoted as A^r_{1jk}) , the radiative rates are almost unchanged with n in a channel. We calculated explicitly the rates of states with $n \leq n_0$. For the states with $n > n_0$, we approximate $A^r_{1jk}(n) = A^r_{1jk}(n_0)$. For $Ar^{14+}(1s^22pnl)^{**} \rightarrow Ar^{14+}(1s^22pn'l')^* + h\nu$ (rate is denoted as A^r_{2jk}), we can calculate the energy-normalized radiative transition matrix elements using eq.(13) and (14). This energy-normalized matrix element varies smoothly with the orbital energy of captured electron[22, 29, 30, 31]. By interpolation, all the energy-normalized matrix elements of infinitely many doubly excited states in a channel can be obtained easily. From the expression (12) and (10), we can obtain all the radiative rates in the channel. In Fig.4, the energy-normalized radiative matrix elements in four channels are plotted, which include $1s^22pns(^3P_0) \rightarrow 1s^22p^2(^3P_1)$, $1s^22pnd(^3P_0) \rightarrow 1s^22p^2(^3P_1)$, $1s^22png(^3F_2) \rightarrow 1s^22p4f(^3D_1)$, $1s^22pnj(^3I_5) \rightarrow 1s^22p7i(^3H_4)$, and n changes from $n = 10$ to $n = \infty$ and continuum states. Each curve varies smoothly with the orbital energy, and all the transition prosesses involving infinitely many high Rydberg states are located in a small energy domain below the threshold value, which can be treated conveniently by interpolation. The radiative rates according to these channels are plotted in Fig.5 and Fig.6. If we assume that our radiative energy-normalized matrix elements are constant and quantum defects can be neglected for high Rydberg states, namely, $\overline{M^r_{jk}}(n) = \overline{M^r_{ji}}(n_0)$ and $\mu_n = 0$ when $n \geq n_0$, we can derive the n^{-3} scaling law $A^r_{2jk}(n) = A^r_{2jk}(n_0) \times (n_0^3\omega_0)/(n^3\omega)$[33, 34, 35] ,here ω is the energy of emitting photon. By analyzing whether the radiative energy-normalized matrix elements $\overline{M^r_{jk}}$ below the threshold value are constant, we can check the validity of n^{-3} scaling law in a channel.

For $1s^22pns(^3P_0) \rightarrow 1s^22p^2(^3P_1)$ and $1s^22pnd(^3P_0) \rightarrow 1s^22p^2(^3P_1)$ channels, $\overline{M^r_{jk}}$ are almost unchanged in the small energy domain below the threshold value as the curves 1 and 2 shown in Fig.4, so n^{-3} scaling law can be well preserved within 1% as shown in Fig.5. However, as angular momentum quantum l increases, the variation of $\overline{M^r_{jk}}$ becomes large in the small energy domain, as shown in Fig.4, and the differences between SRCI method and extrapolating method also become large. For $1s^22png(^3F_2) \rightarrow 1s^22p4f(^3D_1)$ channel, the difference is about 10% as shown in Fig.6(a), and for $1s^22pnj(^3I_5) \rightarrow 1s^22p7i(^3H_4)$, the difference approaches to 80%.

It should be noted that for a certain initial state, the energy-normalized transition matrix element may have nodes, at which the matrix element is equal to zero[39]. In this case, the interpolation should be carried out for the energy-normalized transition elements but not for the radiative rates (i.e., proportional to the square of the transition elements), of course, the n^{-3} scaling law cann't be used in this case.

C. Integrated cross sections

In some works[40, 35], the DR integrated cross sections or rate coefficients have been extrapolated to high Rydberg states directly by n^{-3} scaling law. Because the DR integrated cross sections or rate coefficients are proportional to $P_{ij,k}$ in eq.(13), this extrapolation is equivalent to extrapolating the $P_{ij,k}$ and is also equivalent to extrapolating the dielectronic satellite factors[9, 12, 13, 14]. This extrapolation can only be applied to two cases. One is $A^a_{ji} \ll \sum_k A^r_{jk}$, then we have $A^a_{ji}\sum_k A^r_{jk}/(\sum_{k'} A^r_{jk'} + \sum_{i'} A^a_{ji'}) \simeq A^a_{ji}$ and the n^{-3} scaling law can be used, which often appears in the DR processes for middle or high Z ions. Another is $A^a_{ji} \gg \sum_k A^r_{jk}$ and $\sum_k A^r_{1jk} \ll \sum_k A^r_{2jk}$, then we have $A^a_{ji}\sum_k A^r_{jk}/(\sum_{k'} A^r_{jk'} + \sum_{i'} A^a_{ji'}) \simeq \sum_k A^r_{2jk}$ and the n^{-3} scaling law can be used. For low Z ions, $A^a_{ji} \gg \sum_k A^r_{jk}$ and $A^r_{1jk} \gg \sum_k A^r_{2jk}$, then we have $A^a_{ji}\sum_k A^r_{jk}/(\sum_{k'} A^r_{jk'} + \sum_{i'} A^a_{ji'}) \simeq \sum_k A^r_{1jk} \simeq$ *constant*, so the n^{-3} scaling law cann't be used to DR processes for low Z ions[22, 41], and Karim and Bhalla's conclusion [15] cann't be extended to lower Z ions ($Z <$ 10). For our example, the comparisons of A^a_{ji}, $\sum_k A^r_{1jk}$, $\sum_k A^r_{2jk}$ and $\sum_k A^r_{1jk} + \sum_k A^r_{2jk}$ in four channels are shown in Fig.7 and Fig.8. As n increases, A^a_{ji} and $\sum_k A^r_{2jk}$ (the second type of radiative processes) decrease, but $\sum_k A^r_{1jk}$ (the first type of radiative processes) is almost unchanged. For lower n, $A^a_{ji} \gg \sum_k A^r_{1jk} + \sum_k A^r_{2jk}$ and $\sum_k A^r_{2jk} \gg \sum_k A^r_{1jk}$, as shown in Fig.7 and Fig.8. However, for higher n, $\sum_k A^r_{1jk} \gg \sum_k A^r_{2jk}$, and even for higher l, $\sum_k A^r_{1jk} + \sum_k A^r_{2jk} \gg A^a_{ji}$, as shown in Fig.8, the conditions to extrapolate directly $P_{ij;k}$ cann't be satisfied.

The integrated cross sections S_{ij} in eq.(16) for doubly excited states $1s^22pnd$, $1s^22pnj$ and the sum of $1s^22pnl(l = 1, 2, ..., 11)$ are shown in Fig.9. We compare our results from SRCI method with that from three extrapolations

on the n^{-3} scaling law, including: (1). $A^a_{j_t}$ and A^r_{jk} is extrapolated from $n_0 = 13$; (2). $A^a_{j_t}$ is extrapolated from threshold value and $A^r_{j_t}$ is extrapolated from $n_0 = 13$; (3). $P_{ij;k}$ is extrapolated from $n_0 = 13$. For $1s^22pnd$ resonances, the results from the first and second extrapolations are in good agreements with that from our SRCI method, as shown in Fig.9(a), but the third extrapolation cann't give an agreement, it is because the condition for the third extrapolation hasn't been satisfied, as we have discussed. With the increasing l of $1s^22pnl$ resonances, the differences among the first and second extrapolations and SRCI method become large relatively, as shown in Fig.9(b). However, the main contributions to integrated cross sections come from the resonances with relative small l, so the differences for total integrated cross sections are small among the first and second extrapolations and SRCI method, as shown in Fig.9(c). Above results show that the errors and variations in the calculations of the individual transition probabilities may be large, such as Fig.3 and Fig.5, but because the DR integrated cross sections are proportional to the $P_{ij,k}$, the errors and variations tend to cancel in the evaluation of integrated cross sections[40, 42], we can still obtain good agreements among the SRCI method and first and second extrapolation. But if we extrapolate the $P_{ij,k}$, the errors in $P_{ij,k}$ will affect the cross sections and rate coefficients directly, so we must check the condition before extrapolating $P_{ij,k}$.

The contributions of $1s^22pnl$ resonances with different n and different l are shown in Fig.10. As n increases, the relative contributions of the resonances with high l increase. There are two main reasons. First, for high-n resonances, $Ar^{14+}(1s^22pnl)^{**} \rightarrow Ar^{14+}(1s^22snl)^* + h\nu$ dominates the radiative processes, which is almost non-dependent on l, as shown in Fig.7 and Fig.8; second, the statistical weight g_j in eq.(13) increases with l, which cancels partly the decreasing of $A^a_{j_t}$. These make S_{ij} decrease slowly with l. Generally, the integrated cross section S_{ij} in eq.(13) is a fuction of A^a_{ji}, A^r_{jk} and g_j, which have different dependences on n and l, so when we analyse the integrated cross sections S_{ij} in Fig.10, we must consider their synthetical effects.

D. Rate coefficients

We calculated the rate coefficients for the DR processes of $\Delta N = 0$ transition for Li-like argon. Fig.11(a) shows the theoretical rate coefficients, which is obtained from integrated cross sections folded with the electron beam temperatures ($20\text{meV}/k_B$ transverse temperature and $0.13\text{meV}/k_B$ longitudinal temperature)[43]. Fig.11(b) shows W. Zong et al's experimental measurements[44, 45], where a background of $5 \times 10^{-9} cm^3 s^{-1}$ has been subtracted. The theoretical and experimental line positions compare rather well. In the spectral one can identify Rydberg states up to $n = 18$ for the $1s^22p_{1/2}$ core excitation and $n = 25$ for the $1s^22p_{3/2}$ core excitation, as shown in Fig.11, where we only give labels for a few resonances for simplicity. In general, the theoretical rate coefficients are a little smaller than experimental measurements for high Rydberg states. The possible reasons include that the backgroud is not substracted fully, the contribution of high $l(l \geq 12)$ resonances is ignored, and an extenal field may also give a visible influence on it[46]. We will discuss these effects further in future work.

4. Conclusion

In this paper, a simplified relativistic configuration interaction method is used to study the dielectronic recombination processes. In this method, the infinite resonant doubly excited states involving high Rydberg state can be treated conveniently in a unified mannar by interpolation. This method gives an overall description of all high Rydberg states in a channel, and avoid the inaccuracies of extrapolation through one point. By analyzing the energy-normalized matrix elements in a small energy domain, we can check the validity of extrapolating method based on the widely used n^{-3} scaling laws. In the DR calculation from Li-like to Be-like argon, we found that the respective extrapolations of Auger and radiative rates on n^{-3} scaling laws can give a good results for DR cross sections and rate coefficients, although the difference between extrapolation and SRCI method increases with increasing l in $1s^22pnl$ resonances. However, when we extrapolate $P_{ij;k}$, we must consider the valid condition, otherwise, the errors may be very large. Due to the fully relativistic treatments, our SRCI method can be used to study the DR processes for any Z elements with any elctrons. We will continue to check the validity of scaling law for other system in future.

Acknowledgments

The authors would like to thank Dr. W. Zong to provide us their experimental data and Prof. Fujimoto for his helpful discussions. This work was supported by the Japan Sociaty for Promotion of Science.

References

[1] A. Burgess, Astrophys. J. **139**, 776(1964);

[2] A. V. Vinogradov, I. Yu. Skobelev and E. A. Yukov, Sov. Phys. JETP **45**, 925 (1977).

[3] J. Dubau, A. H. Gabriel, M. Loulergue. L. Steenman-Clark and S. Volone, Mon. Not. R. Astr. Soc **195**, 705(1981).

[4] W. Eissner and M. J. Seaton, J. Phys. B **6**, 2187(1972).

[5] D. R. Flower and J. M. Launay, J. Phys. B **5**, L207(1972).

[6] H. E. Saraph and M. J. Seaton, Phil Trans. Roy. Soc., **A271**, 1(1971).

[7] J Dubau, Ph. D. Thesis, 1973, University of London.

[8] Y. Hahn, Phys. Rev. A **22**, 2896(1980).

[9] D. J. McLaughlin and Y. Hahn, Phys. Rev. A **29**, 712(1984).

[10] M. H. Chen, Phys. Rev. A **31**, 1449(1985).

[11] H. P. Saha, Phys. Rev. A **49**, 894(1994).

[12] e.g. M. H. Chen. Phys. Rev. A **33**, 994(1986). J. Dubau, A.H.Gabriel, M.Loulergue, L.Steennan-Clark, S.Volonte, Mon. Not.. R. ast. Soc **195**, 705(1981).

[13] K. R. Karim and C. P. Bhalla, Phys. Rev. A **37**, 2599(1988).

[14] J. Nilson, J. Quant Spectras. Radiat Transfer **36**, 539(1986).

[15] K. R. Karim, and C. P. Bhalla, Phys. Rev. A **43**, 615 (1991).

[16] M. Gailitis, Sov.Phys.-JETP **17**,1328 (1963).

[17] U. Fano, J. Opt. Soc. Am. **65**,979(1975).

[18] M.J. Seaton, Proc. Phys. Soc. Lond.,**88**,801(1966); Rep. Prog. Phys.,**46**,167(1983).

[19] M.J. Seaton and P.J. Storey, 1976,in Atomic processes and applications, edited by P.G. Burke and B.L. Moiseiwitsch, p.133(North-Holland Publishing Company).

[20] J. Dubau and S. Volonte, Rep. Prog. Phys.,**43**,167(1980).

[21] R.H. Bell and M.J. Seaton, J. Phys. B: At.Mol.Phys. bf 18,1589(1985).

[22] Jian-Guo Wang, Yi-Zhi Qu and Jia-Ming Li, Phys. Rev. A **52**, 4274(1995).

[23] Jian-Guo Wang, Yu Zou, Chen-Zhong Dong and Jia-Ming Li, Chin. Phys. Lett. **12**, 530(1995).

[24] Chen-zhong Dong, Yu Zou, Jian-Guo Wang and Jia-Ming Li, Acta Phys. Sin. **44**, 1712(1995).

[25] Zhong-Xin Zhao and Jia-Ming Li, Acta Phys. Sin. **34**, 1469(1985).

[26] Jia-Ming Li and Zhong-Xing Zhao, Acta Phys. Sini. **31**, 97(1982).

[27] D. A. Liberman, D. T. Cromer and J. T. Waber, Comput. Phys. Commun. **2**, 107(1971).

[28] R. D. Cowan, 1981, the theory of atomic structure and spectra, p.227 (University of California Press).

[29] Lei Liu and Jia-Ming Li, Acta Phys. Sin. **42**, 1901(1993).

[30] Jian-Guo Wang, Xiao-Ming Tong and Jia-Ming Li, Acta Phys. Sin. **45**, 13(1996), see also Yi-Zhi Qu, Jian-Guo Wang, and Jia-Ming Li, Acta Phys. Sin. **46**, 249(1997).

[31] Cheng Zhu, Jian-Guo Wang, Yi-Zhi Qu and Jia-Ming Li, Phys. Rev. A **57**, 1747(1998).

[32] C. M. Lee (Jia-Ming Li), Phys. Rev. A **10**, 584(1974).

[33] K. Moribayashi, and T. Kato, NIFS-DATA-36(1996).

[34] K. Moribayashi, and T. Kato, Physica Scripta **55**, 286(1997).

[35] A. Peleg, E. Behar, P. Mandelbaum, and J.L. Schwob, Phys. Rev. A **57**, 3493(1998)

[36] M.J. Seaton, M.N.R.A.S. **119**, 81(1959).

[37] T. Fujimoto, T. Kato, and Y. Nakamura, IPPJ-AM-23 (1982)

[38] C.J. Romanik, Astrophysics Journal **330**,1022(1988)

[39] e.g., X.L.Liang, J.M.Li, Acta Phisica Sinica **34**, 1479(1985);
M.S.Wang, R.H.Pratt, Phys. Rev. A **29**, 174(1984);
R.Y.Yin, R.H.Pratt, Phys. Rev. A **35**, 1154(1987);
X.M.Tong, L.Yang, J.M.Li, Acta Phis. Sin. **38**, 407(1989).

[40] Y. Hahn, Adv. At. Mol. Phys. **21**, 123(1985).

[41] Yi-Zhi Qu, Jian-Guo Wang, Jian-Kui Yuan and Jia-Ming Li, Phys. Rev. **A 57**, 1033 (1998).

[42] Y. Hahn, Rep. Prog. Phys. 60(1997)691.

[43] G. Kilgus, D. Habs, D. Schwalm, A. Wolf, N. R. Badnell, and A. Muller, Phys. Rev. A **46**, 5730(1992).

[44] W. Zong, R. Schuch, E. Lindroth, H. Gao, D. R. DeWitt, S. Asp, and H. Danared, Phys. Rev. A **56**, 5730(1997).

[45] R. Schuch, D. R. DeWitt, H. Gao, S. Mannervik, W. Zong, and N. R. Basnell, Physica Scripta **T73**, 114(1997).

[46] S. Schennach, A. Muller, O. Uwira, J. Haselbauer, W. Spies, A. Frank, M. Wagner, R. Becker, M. Kleinod, E. Jennewein, N. Angert, P. H. Mokler, N. R. Badnell, and M. S. Pindzola, Z. Phys. D **30**, 291(1994).

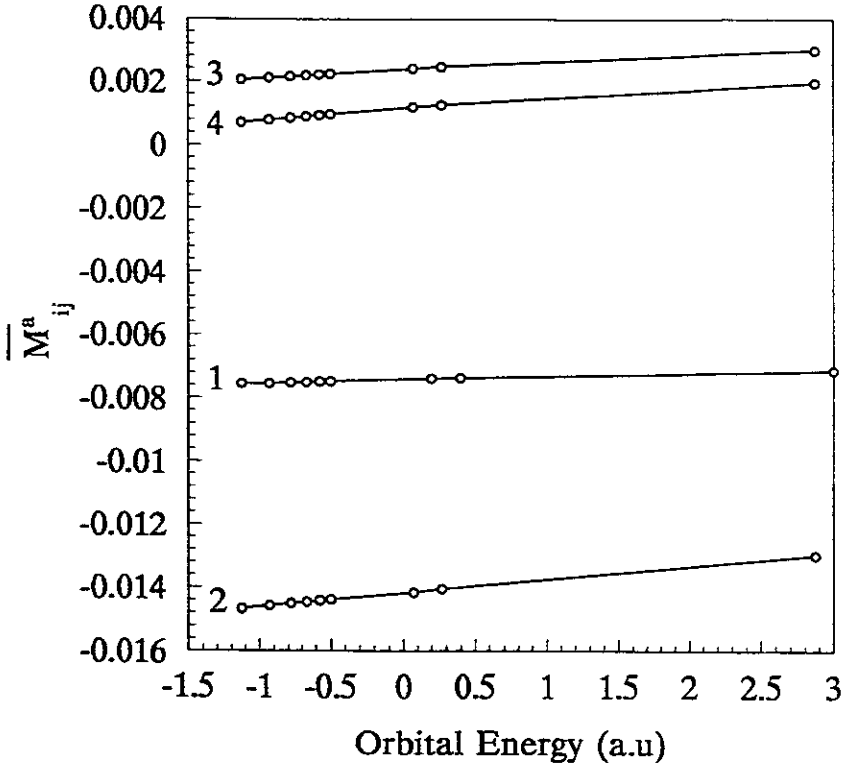

Fig.1 Energy-normalized Auger matrix elements in four channels as a function of orbital energy. 1. $1s^22pns(^3P_0) \rightarrow 1s^22s+\varepsilon p_{1/2}$; 2. $1s^22pnd(^3P_0) \rightarrow 1s^22s+\varepsilon p_{1/2}$; 3. $1s^22png(^3F_2) \rightarrow 1s^22s+\varepsilon p_{3/2}$; 4. $1s^22pnj(^3I_{11}) \rightarrow 1s^22s+\varepsilon g_{9/2}$. Circles are benchmark points, which are calculated explicitly (The circles in following Fig.s are same).

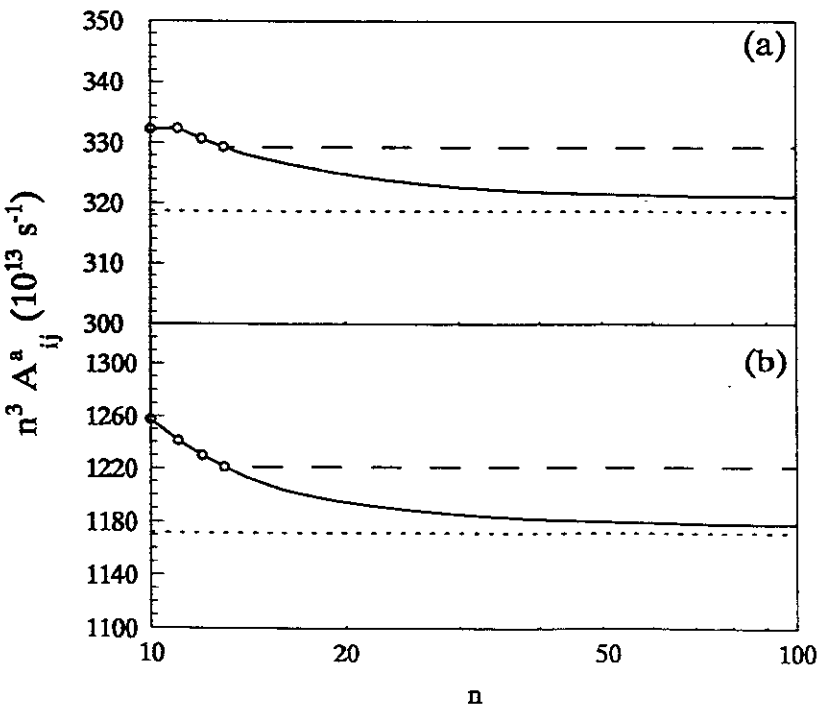

Fig.2 Auger rates multiplied by n^3 in two channels as a function on n. "—": interpolation on SRCI method; "– –": extrapolation from $n_0 = 13$; "· · ·": extrapolation from threshold value. (a). $1s^22pns(^3P_0) \rightarrow 1s^22s+\varepsilon p_{1/2}$; (b). $1s^22pnd(^3P_0) \rightarrow 1s^22s+\varepsilon p_{1/2}$.

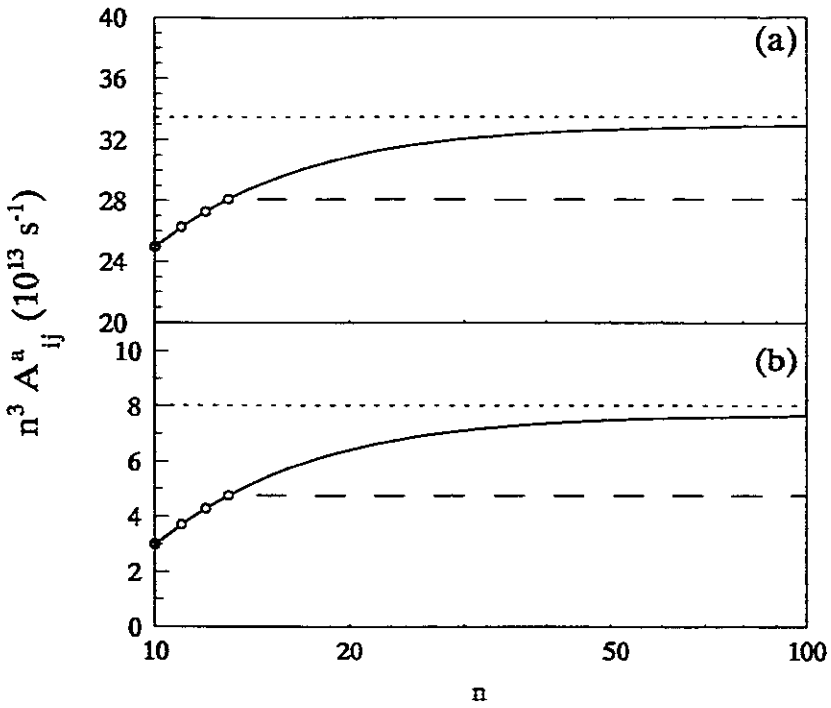

Fig.3 Auger rates multiplied by n^3 in two channels as a function on n. "—": interpolation on SRCI method; "– –": extrapolation from $n_0 = 13$; ". . .": extrapolation from threshold value. (a). $1s^2 2png(^3F_2) \rightarrow 1s^2 2s + \varepsilon p_{3/2}$; (b). $1s^2 2pnj(^3I_{11}) \rightarrow 1s^2 2s + \varepsilon g_{9/2}$.

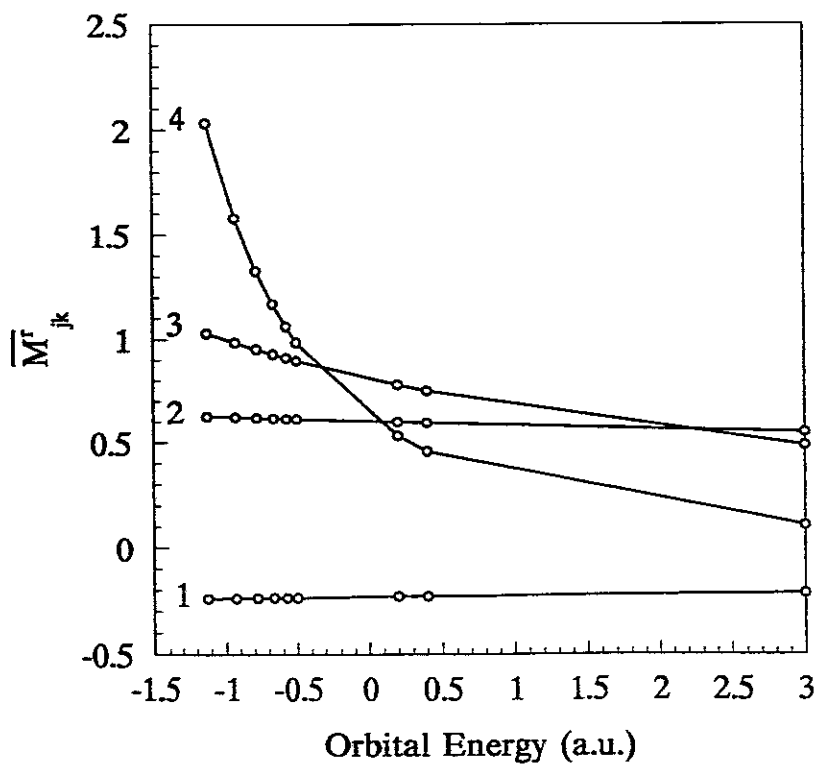

Fig.4 Energy-normalized radiative transition matrix elements in four channels as a function of orbital energy. 1. $1s^2 2pns(^3P_0) \rightarrow 1s^2 2p^2(^3P_1)$; 2. $1s^2 2pnd(^3P_0) \rightarrow 1s^2 2p^2(^3P_1)$; 3. $1s^2 2png(^3F_2) \rightarrow 1s^2 2p4f(^3D_1)$; 4. $1s^2 2pnj(^3I_5) \rightarrow 1s^2 2p7i(^3H_4)$

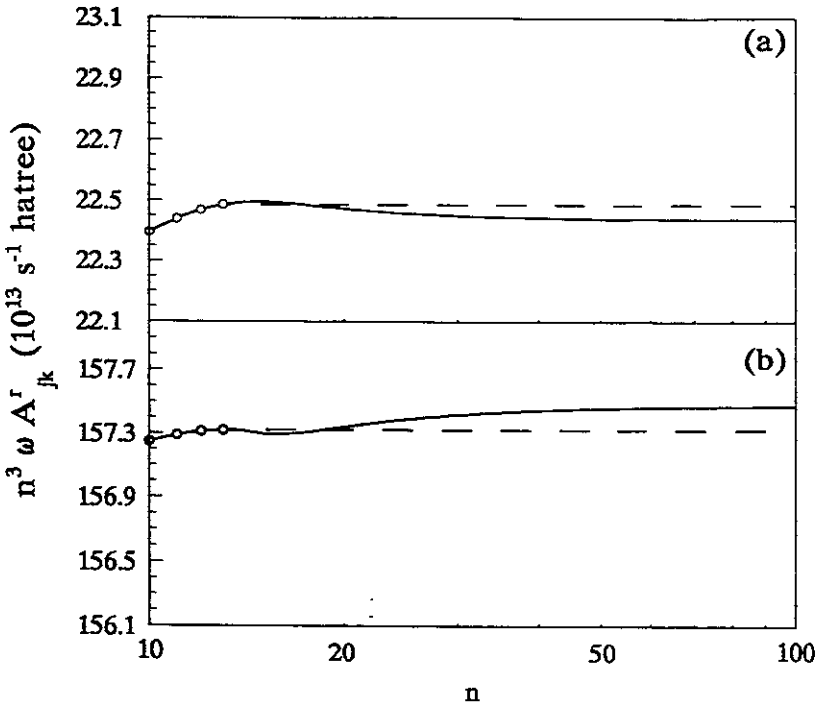

Fig.5 Radiative transition rates multiplied by n^3 in two channels as a function on n. "—": interpolation on SRCI method; "– –": extrapolation from $n_0 = 13$. (a). $1s^2 2pns(^3P_0) \rightarrow 1s^2 2p^2(^3P_1)$; (b). $1s^2 2pnd(^3P_0) \rightarrow 1s^2 2p^2(^3P_1)$

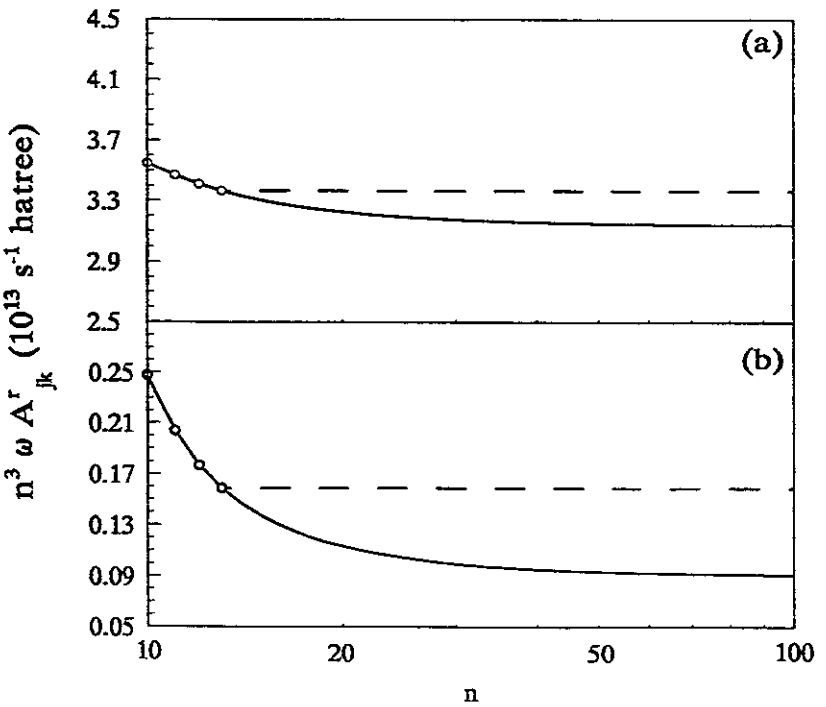

Fig.6 Radiative transition rates multiplied by n^3 in two channels as a function on n. "—": interpolation on SRCI method; "– –": extrapolation from $n_0 = 13$. (a). $1s^2 2png(^3F_2) \rightarrow 1s^2 2p4f(^3D_1)$; (b). $1s^2 2pnj(^3I_5) \rightarrow 1s^2 2p7i(^3H_4)$

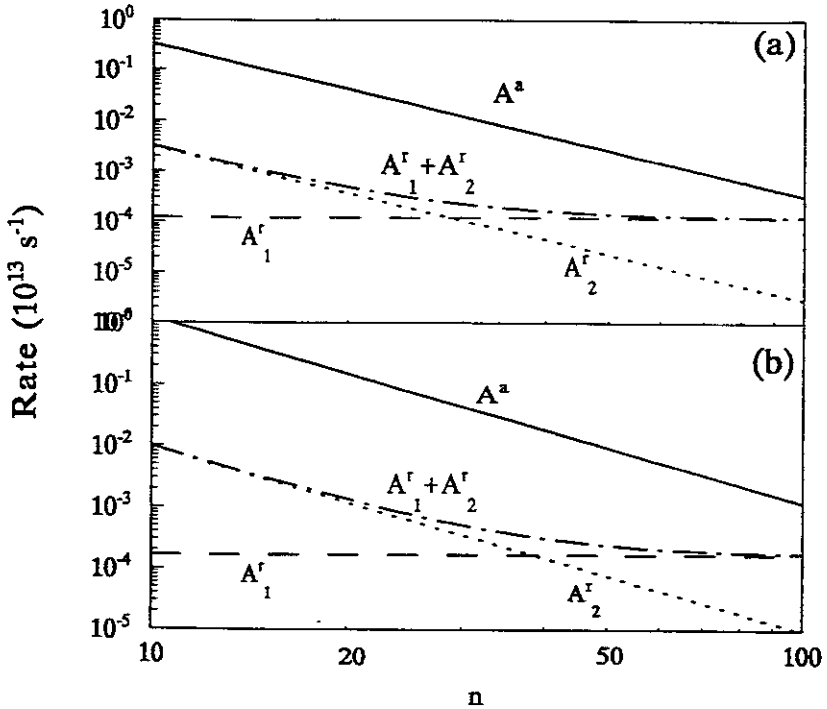

Fig.7 Auger and radiative rates in two channels as a function of n. "—": Auger rates; "– –": radiative transition rates for $Ar^{14+}(1s^22pnl)^{**} \rightarrow Ar^{14+}(1s^22snl)^* + h\nu$; "···": radiative transition rates for $Ar^{14+}(1s^22pnl)^{**} \rightarrow Ar^{14+}(1s^22pn'l')^* + h\nu$; "– · –": sum of above radiative transition rates. (a). $1s^22pns(^3P_0)$ channel; (b). $1s^22pnd(^3P_0)$ channel

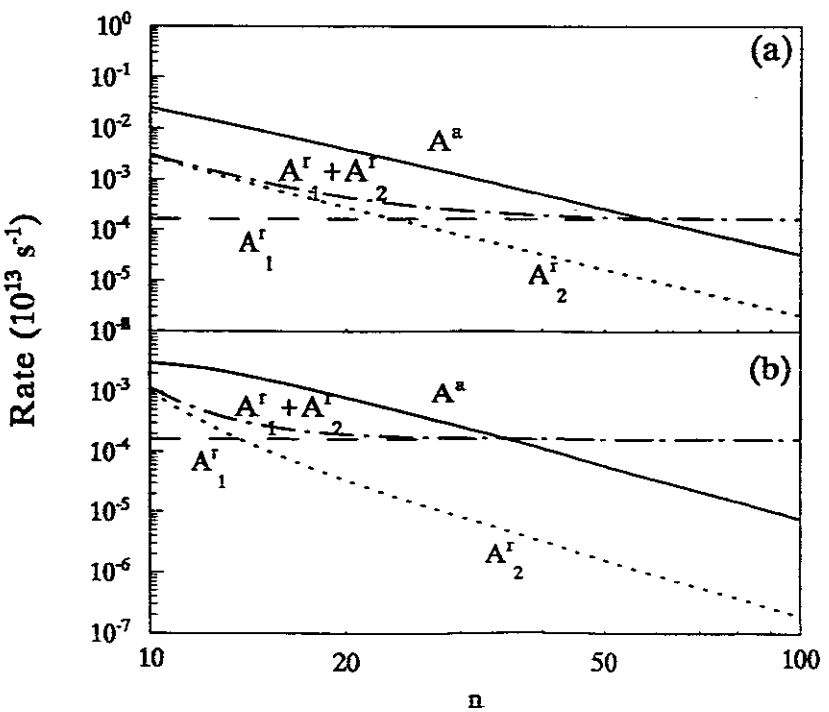

Fig.8 Auger and radiative rates in two channels as a function of n. "—": Auger rates; "– –": radiative transition rates for $Ar^{14+}(1s^22pnl)^{**} \rightarrow Ar^{14+}(1s^22snl)^* + h\nu$; "···": radiative transition rates for $Ar^{14+}(1s^22pnl)^{**} \rightarrow Ar^{14+}(1s^22pn'l')^* + h\nu$; "– · –": sum of above radiative transition rates. and same as (a). $1s^22png(^3F_2)$ channel; (b). $1s^22pnj(^3I_5)$ channel

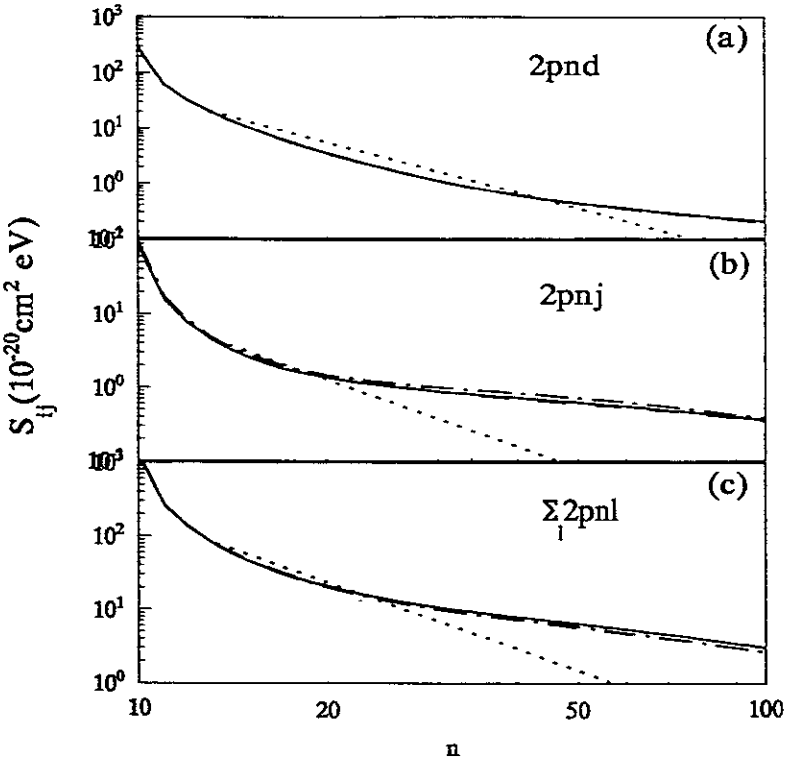

Fig.9 Integrated cross sections for different doubly excited states as a function of n. "—": interpolation on SRCI method; "– –": extrapolation of $A^a(n = 13)$ and $A^r(n = 13)$; "– · –": extrapolation of A^a (threshold value) and $A^r(n = 13)$; "· · ·": extrapolation of $P_{ij;k}$. (a). $1s^2 2pns$; (b). $1s^2 2pnj$; (c). sum of $1s^2 2pnl(l = 1, 2, ..., 11)$

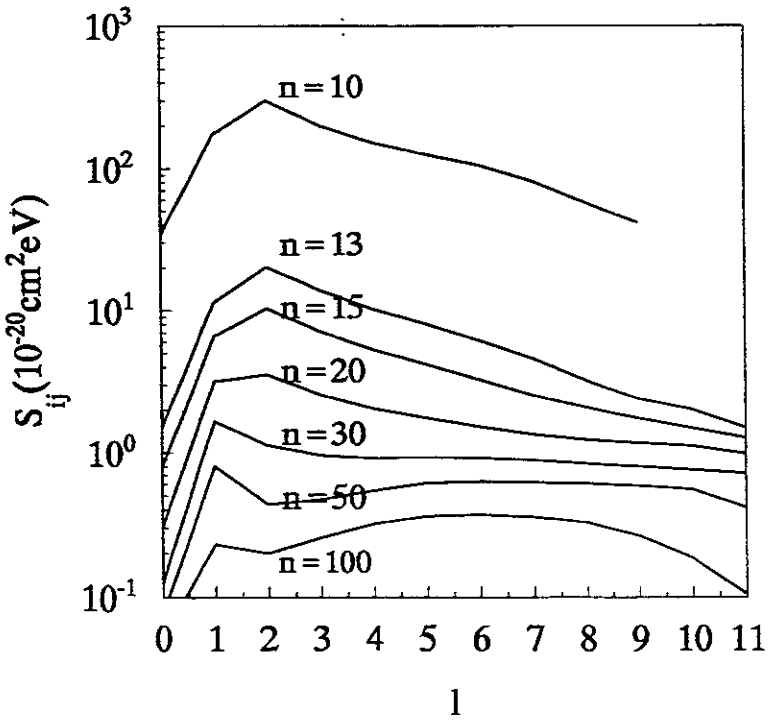

Fig.10 Integrated cross sections with different n for resonances $1s^2 2pnl$ as a function of l.

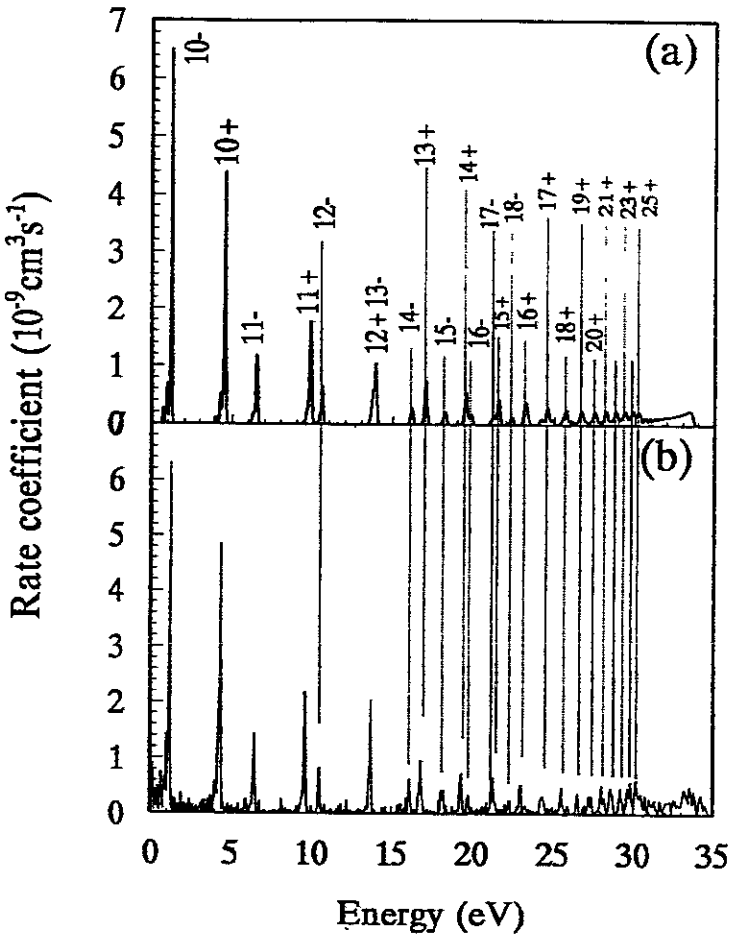

Fig.11 DR rate coefficients as a function of relative energy. "-": $1s^22p_{1/2}$ core excitation; "+": $1s^22p_{3/2}$ core excitation. (a). Theoretical results on SRCI method (folded with 20meV/k_B transverse temperature and 0.13meV/k_B longitudinal temperature); (b). Experimental measurements[44] (a background of $5 \times 10^{-9} cm^3 s^{-1}$ has been subtracted).

Publication List of NIFS-DATA Series

NIFS-DATA-1 Y. Yamamura, T. Takiguchi and H. Tawara,
Data Compilation of Angular Distributions of Sputtered Atoms; Jan 1990

NIFS-DATA-2 T. Kato, J. Lang and K. E. Berrington,
Intensity Ratios of Emission Lines from OV Ions for Temperature and Density Diagnostics ; Mar 1990 [At Data and Nucl Data Tables 44(1990)133]

NIFS-DATA-3 T. Kaneko,
Partial Electronic Straggling Cross Sections of Atoms for Protons; Mar. 1990

NIFS-DATA-4 T. Fujimoto, K. Sawada and K. Takahata,
Cross Section for Production of Excited Hydrogen Atoms Following Dissociative Excitation of Molecular Hydrogen by Electron Impact ; Mar. 1990

NIFS-DATA-5 H. Tawara,
Some Electron Detachment Data for H^- Ions in Collisions with Electrons, Ions, Atoms and Molecules – an Alternative Approach to High Energy Neutral Beam Production for Plasma Heating–;Apr. 1990

NIFS-DATA-6 H. Tawara, Y. Itikawa, H. Nishimura, H. Tanaka and Y. Nakamura,
Collision Data Involving Hydro-Carbon Molecules ; July 1990 [Supplement to Nucl. Fusion 2(1992)25; Atomic and Molecular Processes in Magnetic Fusion Edge Plasmas (Plenum, 1995) p461]

NIFS-DATA-7 H.Tawara,
Bibliography on Electron Transfer Processes in Ion-Ion/Atom/Molecule Collisions –Updated 1990–; Aug. 1990

NIFS-DATA-8 U.I.Safronova, T.Kato, K.Masai, L.A.Vainshtein and A.S.Shlyapzeva,
Excitation Collision Strengths, Cross Sections and Rate Coefficients for OV, SiXI, FeXXIII, MoXXXIX by Electron Impact ($1s^22s^2$-$1s^22s2p$-$1s^22p^2$ Transitions) Dec.1990

NIFS-DATA-9 T.Kaneko,
Partial and Total Electronic Stopping Cross Sections of Atoms and Solids for Protons; Dec. 1990

NIFS-DATA-10 K.Shima, N.Kuno, M.Yamanouchi and H.Tawara,
Equilibrium Charge Fraction of Ions of Z=4-92 (0.02-6 MeV/u) and Z=4-20 (Up to 40 MeV/u) Emerging from a Carbon Foil; Jan.1991 [AT.Data and Nucl. Data Tables 51(1992)173]

NIFS-DATA-11 T. Kaneko, T. Nishihara, T. Taguchi, K. Nakagawa, M. Murakami, M. Hosono, S. Matsushita, K. Hayase, M.Moriya, Y.Matsukuma, K.Miura and Hiro Tawara,
Partial and Total Electronic StoppingCross Sections of Atoms for a Singly Charged Helium Ion: Part 1; Mar. 1991

NIFS-DATA-12 Hiro Tawara,
Total and Partial Cross Sections of Electron Transfer Processes for Be^{q+} and B^{q+} Ions in Collisions with H, H_2 and He Gas Targets -Status in 1991-; June 1991

NIFS-DATA-13 T. Kaneko, M. Nishikori, N. Yamato, T Fukushima, T. Fujikawa, S. Fujita, K. Miki, Y. Mitsunobu, K. Yasuhara, H. Yoshida and Hiro Tawara,
Partial and Total Electronic Stopping Cross Sections of Atoms for a Singly Charged Helium Ion : Part II; Aug. 1991

NIFS-DATA-14 T. Kato, K. Masai and M. Arnaud,
Comparison of Ionization Rate Coefficients of Ions from Hydrogen through Nickel ; Sep. 1991

NIFS-DATA-15 T. Kato, Y. Itikawa and K. Sakimoto,
Compilation of Excitation Cross Sections for He Atoms by Electron Impact; Mar. 1992

NIFS-DATA-16 T. Fujimoto, F. Koike, K. Sakimoto, R. Okasaka, K. Kawasaki, K. Takiyama, T. Oda and T. Kato,
Atomic Processes Relevant to Polarization Plasma Spectroscopy ; Apr. 1992

NIFS-DATA-17 H. Tawara,

Electron Stripping Cross Sections for Light Impurity Ions in Colliding with Atomic Hydrogens Relevant to Fusion Research; Apr. 1992

NIFS-DATA-18 T. Kato,
Electron Impact Excitation Cross Sections and Effective Collision Strengths of N Atom and N-Like Ions -A Review of Available Data and Recommendations- ; Sep. 1992 [Atomic Data and Nuclear Data Tables, 57, 181-214 (1994)]

NIFS-DATA-19 Hiro Tawara,
Atomic and Molecular Data for H_2O, CO & CO_2 Relevant to Edge Plasma Impurities, Oct. 1992

NIFS-DATA-20 Hiro. Tawara,
Bibliography on Electron Transfer Processes in Ion-Ion/Atom/Molecule Collisions -Updated 1993-; Apr. 1993

NIFS-DATA-21 J. Dubau and T. Kato,
Dielectronic Recombination Rate Coefficients to the Excited States of C I from C II; Aug. 1994

NIFS-DATA-22 T. Kawamura, T. Ono, Y. Yamamura,
Simulation Calculations of Physical Sputtering and Reflection Coefficient of Plasma-Irradiated Carbon Surface; Aug. 1994 [J. Nucl. Mater., 220 (1995) 1010]

NIFS-DATA-23 Y. Yamamura and H. Tawara,
Energy Dependence of Ion-Induced Sputtering Yields from Monoatomic Solids at Normal Incidence; Mar. 1995 [At. Data and Nucl. Data Tables, 62 (1996) 149]

NIFS-DATA-24 T. Kato, U. Safronova, A. Shlyaptseva, M. Cornille, J. Dubau,
Comparison of the Satellite Lines of H-like and He-like Spectra; Apr. 1995 [Atomic Data and Nuclear Data Tables, 67., 225 (1997)]

NIFS-DATA-25 H. Tawara,
Roles of Atomic and Molecular Processes in Fusion Plasma Researches - from the cradle (plasma production) to the grave (after-burning) -; May 1995

NIFS-DATA-26 N. Toshima and H. Tawara
Excitation, Ionization, and Electron Capture Cross Sections of Atomic Hydrogen in Collisions with Multiply Charged Ions; July 1995

NIFS-DATA-27 V.P. Shevelko, H. Tawara and E.Salzborn,
Multiple-Ionization Cross Sections of Atoms and Positive Ions by Electron Impact; July 1995 [Suppl. Nucl. Fusion, 6 (1996) 101]

NIFS-DATA-28 V.P. Shevelko and H. Tawara,
Cross Sections for Electron-Impact Induced Transitions Between Excited States in He: n, n'=2,3 and 4; Aug. 1995 [Suppl. Nucl. Fusion, 6 (1996) 27]

NIFS-DATA-29 U.I. Safronova, M.S. Safronova and T. Kato,
Cross Sections and Rate Coefficients for Excitation of $\Delta n = 1$ Transitions in Li-like Ions with $6<Z<42$; Sep. 1995 [Physica Scripta, 54, 68-84 (1996)]

NIFS-DATA-30 T. Nishikawa, T. Kawachi, K. Nishihara and T. Fujimoto,
Recommended Atomic Data for Collisional-Radiative Model of Li-like Ions and Gain Calculation for Li-like Al Ions in the Recombining Plasma; Sep. 1995

NIFS-DATA-31 Y. Yamamura, K. Sakaoka and H. Tawara,
Computer Simulation and Data Compilation of Sputtering Yield by Hydrogen Isotopes ($^1H^+$, $^2D^+$, $^3T^+$) and Helium ($^4He^+$) Ion Impact from Monatomic Solids at Normal Incidence; Oct. 1995

NIFS-DATA-32 T. Kato, U. Safronova and M. Ohira,
Dielectronic Recombination Rate Coefficients to the Excited States of CII from CIII; Feb. 1996 [Physica Scripta, 53, 461-472 (1996), Physica Scripta, 55, 185-199 (1997)]

NIFS-DATA-33 K.J. Snowdon and H. Tawara,
Low Energy Molecule-Surface Interaction Processes of Relevance to Next-Generation Fusion Devices;

Mar. 1996 [Comm. At. Mol. Opt. Phys. 34 (1998) 21]

NIFS-DATA-34 T. Ono, T. Kawamura, K. Ishii and Y. Yamamura,
Sputtering Yield Formula for B_4C Irradiated with Monoenergetic Ions at Normal Incidence; Apr. 1996 [J. Nucl. Mater., 232 (1996) 52]

NIFS-DATA-35 I. Murakami, T. Kato and J. Dubau,
UV and X-Ray Spectral Lines of Be-Like Fe Ion for Plasma Diagnostics; Apr. 1996 [Physica Scripta, 54, 463-470 (1996)]

NIFS-DATA-36 K. Moribayashi and T. Kato,
Dielectronic Recombination of Be-like Fe Ion; Apr. 1996 [Physca Scripta. Vol.55, 286-297 (1997)]

NIFS-DATA-37 U. Safronova, T. Kato and M. Ohira,
Dielectronic Recombination Rate Coefficients to the Excited States of CIII from CIV; July 1996 [J. Quant. Spectrosc. Radiat. Transfer, 58, 193 - 215, (1997)]

NIFS-DATA-38 T. Fujimoto, H. Sahara, G. Csanak and S. Grabbe,
Atomic States and Collisional Relaxation in Plasma Polarization Spectroscopy: Axially Symmetric Case; Oct. 1996

NIFS-DATA-39 H. Tawara (Ed.)
Present Status on Atomic and Molecular Data Relevant to Fusion Plasma Diagnostics and Modeling; Jan. 1997

NIFS-DATA-40 Inga Yu. Tolstikhina,
LS-Averaged 1/Z Method as a Tool of Studying the Interactions of Highly Charged Ions with a Metal Surface; Jan. 1997

NIFS-DATA-41 K. Moribayashi and T. Kato,
Atomic Nuclear Charge Scaling for Dielectronic Recombination to Be-like Ions; Apr 1997

NIFS-DATA-42 H. Tawara,
Bibliography on Electron Transfer Processes in Ion-ion / Atom / Molecule Collisions -Updated 1997 -; May 1997

NIFS-DATA-43 M. Goto and T. Fujimoto,
Collisional-radiative Model for Neutral Helium in Plasma: Excitation Cross Section and Singlet-triplet Wavefunction Mixing; Oct. 1997

NIFS-DATA-44 J. Dubau, T. Kato and U.I. Safronova,
Dielectronic Recombination Rate Coefficients to the Excited States of CI From CII;Jan. 1998

NIFS-DATA-45 Y. Yamamura, W. Takeuchi and T. Kawamura,
The Screening Length of Interatomic Potential in Atomic Collisions; Mar. 1998

NIFS-DATA-46 T. Kenmotsu, T. Kawamura, T. Ono and Y. Yamamura,
Dynamical Simulation for Sputtering of B4C; Mar. 1998

NIFS-DATA-47 I. Murakami, K. Moribayashi and T. Kato,
Effect of Recombination Processes on FeXXIII Line Intensities; May 1998

NIFS-DATA-48 Zhijie Li, T. Kenmotsu, T. Kawamura, T. Ono and Y. Yamamura,
Sputtering Yield Calculations Using an Interatomic Potential with the Shell Effect and a New Local Model; Oct 1998

NIFS-DATA-49 S Sasaki, M. Goto, T. Kato and S. Takamura,
Line Intensity Ratios of Helium Atom in an Ionizing Plasma;Oct 1998

NIFS-DATA-50 I. Murakami, T. Kato and U. Safronova,
Spectral Line Intensities of NeVII for Non-equilibrium Ionization Plasma Including Dielectronic Recombination Processses; Jan. 1999

NIFS-DATA-51 Hiro Tawara and Masa Kato,
Electron Impact Ionization Data for Atoms and Ions -up-dated in 1998-;Feb. 1999

NIFS-DATA-52 J.G. Wang, T. Kato and I. Murakami,
Validity of n^{-3} Scaling Law in Dielectronic Recombination Processes; Apr. 1999